Structure and Function of BcpE2, the Most Promiscuous GH3-Family Glucose Scavenging Beta-Glucosidase

Benoit Deflandre,[a] Cédric Jadot,[a] Sören Planckaert,[b] Noémie Thiébaut,[a] Nudzejma Stulanovic,[a] Raphaël Herman,[a] Bart Devreese,[b] Frédéric Kerff,[a] Sébastien Rigali[a]

aInBioS – Center for Protein Engineering, Institut de Chimie B6a, University of Liège, Liège, Belgium
bLaboratory for Microbiology, Department of Biochemistry and Microbiology, Ghent University, Ghent, Belgium

Frédéric Kerff and Sébastien Rigali jointly supervised this work.

ABSTRACT Cellulose being the most abundant polysaccharide on earth, beta-glucosidases hydrolyzing cello-oligosaccharides are key enzymes to fuel glycolysis in microorganisms developing on plant material. In *Streptomyces scabiei*, the causative agent of common scab in root and tuber crops, a genetic compensation phenomenon safeguards the loss of the gene encoding the cello-oligosaccharide hydrolase BglC by awakening the expression of alternative beta-glucosidases. Here, we revealed that the BglC compensating enzyme BcpE2 was the GH3-family beta-glucosidase that displayed the highest reported substrate promiscuity and was able to release the glucose moiety of all tested types of plant-derived heterosides (aryl β-glucosides, monolignol glucosides, cyanogenic glucosides, anthocyanosides, and coumarin heterosides). BcpE2 structure analysis highlighted a large cavity in the PA14 domain that covered the active site, and the high flexibility of this domain would allow proper adjustment of this cavity for disparate heterosides. The exceptional substrate promiscuity of BcpE2 provides microorganisms a versatile tool for scavenging glucose from plant-derived nutrients that widely vary in size and structure. Importantly, scopolin was the only substrate commonly hydrolyzed by both BglC and BcpE2, thereby generating the potent virulence inhibitor scopoletin. Next to fueling glycolysis, both enzymes would also fine-tune the strength of virulence.

IMPORTANCE Plant decaying biomass is the most abundant provider of carbon sources for soil-dwelling microorganisms. To optimally evolve in such environmental niches, microorganisms possess an arsenal of hydrolytic enzymatic complexes to feed on the various types of polysaccharides, oligosaccharides, and monosaccharides. In this work, structural, enzymatic, and expression studies revealed the existence of a "swiss-army knife" enzyme, BcpE2, that was able to retrieve the glucose moiety of a multitude of plant-derived substrates that vary in size, structure, and origin. This enzyme would provide the microorganisms with a tool that would allow them to find nutrients from any type of plant-derived material.

KEYWORDS enzyme promiscuity, genetic compensation, glycosyl hydrolase, carbon metabolism, host-pathogen interaction, plant heterosides

The major source of soil organic carbon derives from plant senescence, with cellulose, xylan, starch, and lignin being the most abundant naturally-occurring carbon-containing polymers. Optimal colonization of carbon-rich environments, thus, mainly relies on the ability of microorganisms to participate and feed on decomposing plant biomass. The same rationale applies to phytopathogenic bacteria for which the energy required for plant colonization must be supported by catabolic pathways biased toward carbon source utilization. Filamentous Gram-positive bacteria of the genus *Streptomyces* are well-known for their role in soil mineralization and their capability to consume

diverse polysaccharides, oligosaccharides, and monosaccharides (1–4). Given that cellulose is the most abundant polysaccharide on earth, the acquisition of a complete cellulolytic system provides a competitive advantage in organic environments. However, as cellobiose is the main product resulting from cellulolysis (5, 6), possessing the CebEFG-MsiK cello-oligosaccharide transporter (7–9) and the beta-glucosidase BglC (10, 11) for their subsequent hydrolysis into glucose, would be a sufficient requirement for the survival of streptomycetes within a microbial community consuming plant material (2).

For *Streptomyces scabiei*, the bacterium responsible for common scab in root and tuber crops, cellobiose and cellotriose are of particular importance. Indeed, their import and subsequent catabolism do not only feed glycolysis with glucose, but they (especially cellotriose (12)) are also the environmental triggers of the onset of its pathogenic lifestyle (7, 12–17). This tight link of cellulose by-product utilization for both primary metabolism and the onset of virulence is perfectly highlighted by the phenotype of the null mutant of gene *scab57721* encoding the β-glucosidase BglC. Indeed, strain *S. scabiei* Δ*bglC* poorly grows when cultured with cellobiose or cellotriose provided as sole carbon sources and displays a hyper-virulent phenotype due to the constitutive production of thaxtomin A, the main virulence determinant (10). Surprisingly, we recently showed that BglC was also able to remove the glucose moiety of the scopolin heteroside (18) produced by plants under host colonization thereby generating scopoletin, a potent inhibitor of thaxtomin A production (19). The hydrolysis of scopolin by BglC displays a substrate inhibition kinetic profile (18) that contrasts with the typical Michaelis-Menten saturation curve observed for the degradation of its natural substrates cellotriose and cellobiose (10). At low scopolin concentration, the generated scopoletin from BglC would compete with the action of the virulence elicitor cellobiose/cellotriose and would reduce thaxtomin A production. Instead, at higher scopolin concentrations the activity of BglC would be limited by a substrate inhibition mechanism which would instead activate the biosynthesis of this main virulence factor. This enzyme has thus different kinetic properties on either the virulence elicitors emanating from the plant host or a molecule produced by the plant defense mechanisms, thereby occupying a key position to fine-tune the production of thaxtomin A (18).

Surprisingly, we showed that the deletion of *bglC* in *S. scabiei* was not lethal when the mutant strain was inoculated on media with cellobiose supplied as a unique carbon source (20). The unexpected survival of the *bglC* null mutant in this culture condition was due to a genetic compensation phenomenon that awakens the expression of the gene *scab2391* encoding an alternative GH1-family β-glucosidase (20). This sugar hydrolase was called BcpE1 (SCAB_2391), BcpE standing for BglC compensating enzyme, and is a paralogue of BglC, both enzymes having catalytic properties in the same order of magnitude toward cellobiose (20). Interestingly, the genetic compensation phenomenon associated with the loss of *bglC* resulted in the overexpression of a second gene (*scab64101*) encoding a GH3-family β-glucosidase called BcpE2 (20). However, in contrast to BcpE1, BcpE2 cannot hydrolyze cellobiose (20). The reason why the *bglC*-dependent mechanism of compensation selected the product of *scab64101* as an alternative β-glucosidase remains unknown. If the role of BcpE2 was not to provide glucose from cellobiose or cellotriose, how could this enzyme compensate for the loss of function of BglC? In other words, how would *S. scabiei* and other streptomycetes benefit from the activation of BcpE2 in their environmental niche?

In this work, we investigated the function of BcpE2 through enzymatic, structural, and expression studies. Our results demonstrated that BcpE2 can release the glucose moiety of various types of plant-derived heterosides. Thanks to its exceptional substrate promiscuity, BcpE2 safeguarded the feeding of glycolysis with glucose hydrolyzed from highly diverse carbon sources. Moreover, BcpE2 also degraded scopolin into scopoletin following a substrate inhibition profile, thereby also compensating for the loss of the function of BglC toward the host defense mechanism.

TABLE 1 Data collection and refinement statistics

Metric	BcpE2 (PDB accession no. 7PJJ)
Data collection	
Wavelength	0.98010
Space group	P 3_1 2 1
a, b, c (Å)	109.62, 109.62, 164.18
α, β, γ (°)	90, 90, 120
Resolution range (Å)[a]	47.4 –3.09 (3.27–3.09)
R_{merge} (%)[a]	27.3 (222)
$I/<\sigma I>$[a]	6.9 (0.9)
Completeness (%)[a]	99.3 (96.6)
Redundancy[a]	6.7 (6.4)
CC 1/2[a]	0.991 (0.301)
Refinement	
Resolution range (Å)[a]	47.4–3.09 (3.2–3.09)
No. of unique reflections[a]	21414 (1981)
R_{work} (%)[a]	22.3 (33.6)
R_{free} (%)[a]	27.0 (35.5)
No. atoms	
Protein	5904
Solvent	14
RMS deviations from ideal stereochemistry	
Bond lengths (Å)	0.009
Bond angles (º)	1.00
Mean B factor (Å^2)	
Protein	90.9
Solvent	94.3
Ramachandran plot	
Favored region (%)	92.7
Allowed regions (%)	6.4
Outlier regions (%)	0.9

[a]Numbers in parenthesis refer to the highest resolution shell.

RESULTS

Structure of BcpE2 of *Streptomyces scabiei*. We obtained the crystallographic structure of BcpE2 at 3.09 Å (Table 1 and Fig. 1). The crystal belongs to the P3$_1$21 space group with one molecule in the asymmetric unit. The BcpE2 structure is characterized by R_{work} and R_{free} values of 22.3% and 27%, respectively (Table 1), and contains residues 10 to 822. Six regions could not be built because of a lack of electron density: the first nine amino acids (AA), the 12 C-terminal residues, which consist of a His$_6$-Tag and a linker, and four loops (residues 70 to 73, 336 to 339, 436 to 443 and 531 to 536). BcpE2 is monomeric and is made of four domains (Fig. 1A and Table 1): an N-terminal (β/α)$_8$ TIM barrel domain (residues 10 to 306), an (α/β)$_6$-sandwich domain (residues 316 to 398 and 551 to 650), a PA14 domain (residues 404 to 548), and a C-terminal fibronectin type III-like (fn3) domain (residues 711 to 821). In addition, a 60 AA linker is present between (α/β)$_6$-sandwich and the fibronectin type III-like domains and mostly runs on the (β/α)$_8$ TIM barrel domain. This architecture was identified in only 19 sequences among all 199 characterized prokaryotic and eukaryotic GH3s by mining the CAZy database. Only two structures, KmBglI from *Kluyveromyces marxianus* (PDB accession no. 3AC0) (21) and DesR from *Streptomyces venezuelae* (PDB accession no. 4I3G) (22), were found with this architecture. While the (β/α)$_8$ TIM barrel, the (α/β)$_6$-sandwich, and the fn3 domains were well superimposed, including the linker preceding the C-terminal domain (root mean square deviation [RMSD] of 0.91 Å over 507 Cα for KmBglI and 0.90 Å over 504 Cα for DesR), the PA14 domain could not be superimposed simultaneously with the three other domains (Fig. 1B and C). In BcpE2 and KmBglI, the
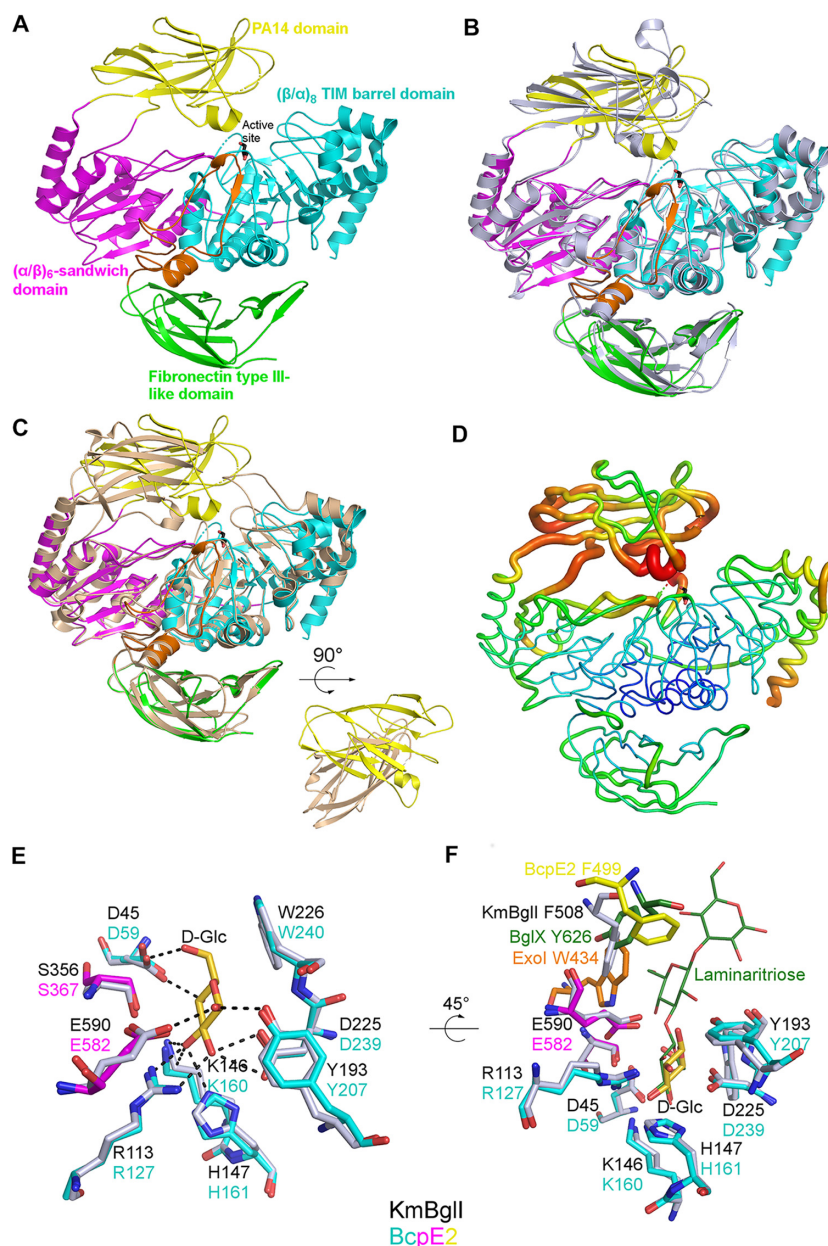
FIG 1 Overall fold and active site description of BcpE2 of *S. scabiei*. (A) Cartoon representation of the BcpE2 structure. The glycerol molecule in the active site (black sticks) results from the cryo-protectant solution used for freezing the crystal. (B) Superimposition of BcpE2 and KmBglI (light blue). (C) Superimposition of BcpE2 and DesR (light orange). Their PA14 is also shown with a 90° rotation to highlight the different orientations. (D) Ribbon representation of BcpE2. The ribbon radius was proportional to the mean B-factor value of the residues and a rainbow coloring scheme (blue low B factor value to red high B-factor value). (E) Superimposition of the catalytic site of BcpE2 (residues are colored by domain with the same coloring scheme as in (B) with KmBglI (gray) in complex with D-Glucose (D-Glc in gold)) in subsite −1. Hydrogen bonds with D-Glc are shown as black dashed lines. (F) Same as (E) but with a 45° rotation and the addition of ExoI (orange) and the BglX:Laminaritriose complex (green) superimposed. The aromatic residues of subsite +1 of KmBglI and BglX are also shown as sticks, as well as their likely equivalent in ExoI and BcpE2. The position of F499 in BcpE2 (yellow sticks) comes from the PA14 domain superimposed independently on the PA14 domain of KmBglI.

orientation was roughly similar, and they were characterized by an RMSD of 2.6 Å over 81 Cα when superimposed independently. In DesR, the PA14 domain was 40 AA shorter than in BcpE2 and approximately perpendicular to the orientation in the latter. When superimposed independently, the RMSD between them was 4.7 Å over 88 Cα. The PA14 domain of BcpE2 was also characterized by B factor values significantly higher than the rest of the protein, particularly in the active site vicinity (Fig. 1D),

indicating the likely flexibility of this domain. This feature was also noted for KmBglI and potentially associated with substrate recognition (21).

The catalytic site of BcpE2. Both KmBglI and DesR have been crystallized with a β-D-glucose molecule present in their active site (-1 subsite) (21–23). This molecule corresponded to the buried end of the substrate, and, in KmBglI, it was found in a pocket made of 9 residues (7 of them being involved in hydrogen bonds) belonging to the $(\alpha/\beta)_8$ TIM barrel and the $(\alpha/\beta)_6$-sandwich domains. These residues, which include the catalytic glutamate and aspartate responsible for the two-step double displacement mechanism (24), were strictly conserved with a very similar orientation in DesR and BcpE2 (RMSD calculated for all nonhydrogen atoms of 0.48 Å and 0.60 Å, respectively; Fig. 1E). Fig. S1 shows the structure-based sequence alignment of BcpE2 with homologous and biochemically characterized proteins (Table S1) that either display the highest structural or primary sequence similarity. The two catalytic residues – Asp239 and Glu582 – were strictly conserved in all homologous GH3s (Fig. S1). These residues provided an ideal geometry to stabilize the five hydroxyl groups of glucose with at least one hydrogen bond and facilitate efficient hydrolysis. The active site of BcpE2 also included Asp59, Arg127, and three additional aromatic AAs, namely, Tyr207, Trp240, and Phe499, which were generally conserved in the closest GH3-family enzymes (Fig. S1).

In KmBglI, Phe508, which belongs to the PA14 domain, had been identified by site-directed mutagenesis as important for substrate hydrolysis and was part of the subsite ($+1$) (21). In BcpE2, Phe499 was equivalent when the two PA14 domains were superimposed independently (Cα 2 Å apart) but was shifted toward the position that the substrate would likely occupy when the entire structures were superimposed (Cα 5 Å apart). This positioning could be the result of the crystal packing and/or the flexibility observed. An aromatic residue at this position seemed to be a common feature in GH3 enzymes but could come from different structural elements (Fig. S1). For example, in the ExoI enzyme from barley (25), it was located on a loop of the $(\alpha/\beta)_6$-sandwich domain. In the dimer forming BglX from *Pseudomonas aeruginosa* (24), it came from an extended loop of the second molecule of the dimer (Fig. 1F). In BcpE2, the high B factor values observed in this region and the likely related flexibility made it difficult to extract additional information about substrate specificity in the ($+1$) subsite at this stage.

Seeking the natural substrate(s) of BcpE2. Earlier work showed that BcpE2 displayed a strong hydrolytic activity on the synthetic chromogenic substrate pNPβG (20), suggesting that the enzyme should target carbohydrates with terminal glucose attached by a β-1,4 linkage. According to the KEGG pathway, BcpE2 of *S. scabiei* 87-22 was suggested as a candidate beta-glucosidase possibly involved in cyanoamino acid metabolism (https://www.genome.jp/kegg-bin/show_pathway?scb00460+SCAB_64101). Two cyanogenic glucosides were, thus, selected as possible targets of BcpE2, i.e., amygdalin and linamarin (Table 2). To help identify other putative substrates that could be hydrolyzed by BcpE2, we generated a phylogenetic tree with BcpE2 of *S. scabiei* and the full-length sequences of the 14 closest characterized bacterial GH3-family β-glucosidases, and with five other characterized bacterial GH3s with lower overall identity but with high query coverage and containing the PA14 domain (Fig. S2).

According to these *in silico* analyses combined with a literature survey, 14 candidate natural substrates were selected for BcpE2 (Table 2). Most of them are β-1,4 linked heterosides commonly found in plants, i.e., compounds with glucose (or another carbohydrate moiety) linked by a glycosidic bond to an aglycone. They belong to different types of plant heterosides with extremely variable aglycone moieties, i.e., (i) aryl-β-glucosides (arbutin, salicin), (ii) monolignol glucosides (p-coumaryl alcohol 4-O-glucoside, syringin, coniferin), (iii) anthocyanosides (cyanin), (iv) coumarin heterosides (esculin, scopolin), and cyanogenic glycosides (linamarin, amygdalin).

The candidate substrates listed in Table 2 were tested to determine the ability of BcpE2 to release their glycosidic moiety (Fig. 2) beta-glucosidase BglC was also included in our enzymatic assays to compare the respective substrate specificities of each enzyme. Both pure six histidine-tagged enzymes were incubated with the candidate substrates and reactions were conducted at their optimal pH (7.5) and temperature (40°C) (optima deduced from

TABLE 2 Overview of the activity of BcpE2 and BglC on selected disaccharides and heterosides

Substrate	Category	TLC assays[a]		Kinetic parameters (BcpE2)			
		BcpE2	BglC	K_m (mM)	K_{cat} (s^{-1})	K_{cat}/K_m (mM$^{-1} \cdot$s^{-1})	K_i (mM)
Cellobiose	Disaccharides (β-1,4 glucose)	−	+	/(20)	/(20)	/(20)	/(20)
Gentiobiose	Disaccharides (β-1,6 glucose)	±/−	±/−	NT	NT	NT	NT
Xylobiose	Disaccharides (β-1,4 xylose)	−	−	NT	NT	NT	NT
Laminaribiose	Disaccharides (β-1,3 glucose)	±	+	6.557 ± 1.410	8.74 ± 1.02	1.33	NA
Salicin	Aryl-β-glucosides	+	±	0.142 ± 0.030	53.20 ± 2.37	375.71	NA
Arbutin	Aryl-β-glucosides	+	±/−	0.367 ± 0.080	43.17 ± 2.50	117.49	NA
Amygdalin	Cyanogenic glycosides	±	−	NT	NT	NT	NT
Linamarin	Cyanogenic glycosides	+	−	NT	NT	NT	NT
Scopolin	Coumarin heterosides	+	+	0.356	191.90	539.65	0.152
Esculin	Coumarin heterosides	+	±	NT	NT	NT	NT
4-MUG	Aryl-β-glucosides	+	+	NT	NT	NT	NT
Cyanin (Cyanidin-3,5-di-O-glucoside)	Antho-cyanosides	+	−	NT	NT	NT	NT
p-coumaryl alcohol 4-O-glucoside	Monolignol glucosides	+	±	0.236	77.15	326.49	0.593
Coniferin	Monolignol glucosides	+	±	0.151 ± 0.043	83.30 ± 5.90	551.29	NA
Syringin	Monolignol glucosides	+	−	0.608 ± 0.166	26.43 ± 3.07	43.46	NA

[a]The TLC assays columns summarize the results displayed in Fig. 2A by the attribution of qualitative hydrolysis scores for the two enzymes. '+' indicates a complete hydrolysis, '±' indicates an incomplete hydrolysis, '±/−' indicates weak hydrolysis, and '−' indicates the absence of substrate hydrolysis (or glucose release). The kinetic parameters columns summarize the measured by initial velocities plotted as a function of the substrate concentration to obtain Henri-Michaelis-Menten or substrate inhibition curves fitted with GraphPad Prism (9.2.0). The error values of the K_m, k_{cat}, and K_i values indicate the extent of the interval to be considered to determine the value with 95% confidence (asymptotic method). Abbreviations: pNPβG: 4-Nitrophenyl β-D-glucopyranoside; 4-MUG: 4-methylumbelliferyl-β-D-glucoside; NT: not tested; NA: not applicable; /, too weak activity for obtaining kinetic parameters (data from reference (20)).

results presented in Fig. S3 for BcpE2 and described in reference (10) for BglC. Reaction samples were spotted on thin-layer chromatography (TLC) plates and migrated in an elution chamber to separate glucose (or other saccharides) from the remainder moieties of the substrate (Fig. 2A).

Cellobiose was first tested as a positive-control and negative-control substrate for BglC and BcpE2, respectively. Indeed, as shown in Fig. 2A, glucose was only released from cellobiose when this substrate is incubated with BglC. Other D-glucose disaccharides were tested, namely, gentiobiose (D-glucose linked in β[1→6]) and laminaribiose (D-glucose linked in β[1→3]). Surprisingly, BglC could efficiently degrade laminaribiose whereas BcpE2 could only partially degrade this substrate. Both enzymes were equally inefficient on gentiobiose where barely perceptible amounts of glucose were released (Fig. 2A). Neither BglC nor BcpE2 was active on xylobiose, suggesting that these enzymes could not properly target D-xylose saccharides.

Strikingly, BcpE2 was revealed to be active on all tested heterosides (Fig. 2A). Complete hydrolysis was observed for (i) the two aryl-β-glucosides salicin and arbutin, (ii) the cyanogenic glucoside linamarin, (iii) the pink/purple anthocyanoside cyanidin-3,5-di-O-glucoside chloride (cyanin), (iv) all three monolignol glucosides syringin, coniferin, and p-coumaryl alcohol 4-O-glucoside, (v) the coumarin heteroside esculin, and (vi) the synthetic substrate 4-MUG (Fig. 2A). Significant yet incomplete hydrolysis by BcpE2 was also observed for the cyanogenic glucoside amygdalin. In contrast, BglC was inactive on most tested heterosides except the synthetic substrate 4-MUG, and scopolin as previously described (18). Only partial substrate hydrolysis by BglC could be observed for esculin, coniferin, p-coumaryl alcohol 4-O-glucoside, and salicin (Fig. 2A). Overall, we observed that the substrate specificity of BcpE2 was broad and often complementary to that of BglC (Table 2). Surprisingly and despite an extensive variability in the aglycone parts of the tested compounds, BcpE2 managed to generate glucose from all the heteroside substrates considered in this study.

After determining the best candidate substrates of BcpE2 by preliminary enzymatic assays on TLC, a subset of them were used to evaluate the kinetic parameters of BcpE2. The values of the Michaelis constant (K_m), catalytic rate constant (or turnover; k_{cat}), and catalytic efficiency (k_{cat}/K_m) were determined for BcpE2 toward the seven following substrates: salicin, arbutin, laminaribiose, syringin, p-coumaryl alcohol glucoside, coniferin, and scopolin (Table 2) based on the nonlinear regressions in Fig. 2B.
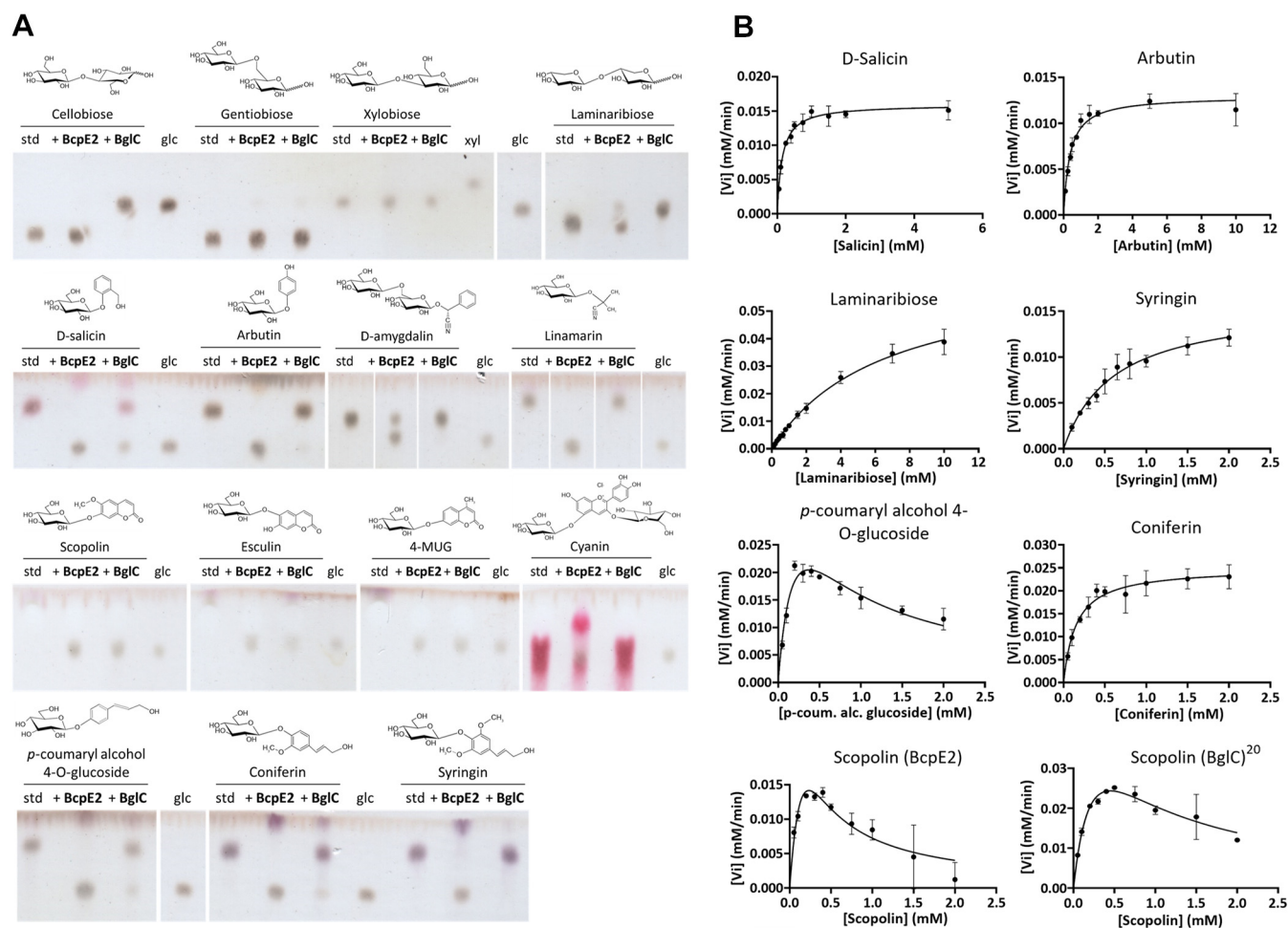
FIG 2 Substrate specificities of BcpE2 and BglC. (A) TLC plates revealed the release of glucose (glc) after incubation of a variety of substrates (5 mM) with BcpE2 or BglC (1 μM) compared to the intact substrate (standard [std]). The chemical structure is displayed above each substrate. Note that for scopolin, esculin, and 4-MUG the substrates are in the solvent front. (B) Nonlinear regressions of the kinetic analyses of BcpE2 toward seven substrates and one for BglC. The initial velocity (V_i, mM/min) was estimated by the rate of glucose released by the enzyme as a function of substrate concentrations (in mM). Individual values were entered into the GraphPad Prism software (9.2.0) which fitted the data to the Henri-Michaelis-Menten model by nonlinear regression. In the case of a decrease of the Vi at high substrate concentrations, the data were fitted to the Substrate Inhibition model. Error bars display the standard deviation values determined for the V_i by three replicates at each substrate concentration.

The best affinity of BcpE2 was – as indicated by the lowest K_m values – observed toward salicin and coniferin with a K_m of about 0.15 mM. The other substrates displayed values on the same order of magnitude, except laminaribiose for which the 6.557 mM estimated K_m value indicates a low affinity of the β-glucosidase for this substrate (as anticipated from assays on TLC plates; Fig. 2A). Regarding the turnover parameter, the monolignol glucoside coniferin was the most efficiently hydrolyzed substrate with a k_{cat} value of 83.3 s^{-1}. This heteroside thus had the highest catalytic efficiency at about 550 mM^{-1} s^{-1}, surpassing salicin and p-coumaryl alcohol glucoside by some margin and was thereby the best-reported substrate for BcpE2.

While most of the tested substrates exhibited conventional Henri-Michaelis-Menten behavior upon hydrolysis by BcpE2, two heterosides revealed substrate inhibition, namely, the p-coumaryl alcohol glucoside and scopolin (Fig. 2B). Indeed, the monolignol glucoside p-coumaryl alcohol glucoside showed a decrease in the initial velocity at high substrate concentration. The calculated inhibition constant (K_i) value for p-coumaryl alcohol glucoside was estimated at 0.6 mM and the theoretical K_m and k_{cat} values without the inhibition phenomenon would be 0.236 mM and 77.15 s^{-1}, respectively. This suggested that this monolignol glucoside was also a good substrate for BcpE2, yet at relatively low concentrations. Interestingly, scopolin was the only natural substrate

to be hydrolyzed by both BcpE2 and BglC in the TLC experiment (Fig. 2A). We, therefore, decided to evaluate their respective kinetic parameters to evaluate how efficiently they degrade this substrate. To obtain similar initial velocity values at low substrate concentrations, a concentration 20-times higher of BglC compared to BcpE2 was required, suggesting a much better k_{cat} for the latter. In addition, as indicated by the aspect of the nonlinear regressions in Fig. 2B, both enzymes were subjected to substrate inhibition. However, the K_i value for BcpE2 appeared to be lower, indicating a stronger inhibition compared to BglC (Table 2).

Production of BcpE2 was induced by the aryl-β-glucoside salicin. To validate the role of BcpE2 in heteroside degradation *in vivo*, it was mandatory to show that BcpE2 was produced when *S. scabiei* encountered these types of molecules in its environment. From all tested substrates that were best hydrolyzed by BcpE2, we chose salicin as a putative natural elicitor of BcpE2 production (also due to its availability in terms of cost and quantity) for our *in vivo* production assays. *S. scabiei* was cultivated under conditions that allow BglC production (minimal medium containing cellobiose) and/or with salicin as a putative trigger for BcpE2 production. The different intracellular crude extracts were separated by anion-exchange chromatography and the fractions obtained were first tested against pNPβG as the substrate to detect those containing β-glucosidases, and then subjected to targeted proteomics for the identification and quantification of BglC and BcpE2. The semiquantitative abundances of BglC and BcpE2 under the three tested culture conditions are presented in Fig. 3.

As previously reported, the production of BglC was triggered by the presence of cellobiose. Salicin was neither able to induce (when provided as a unique carbon source) nor repress (when in combination with cellobiose) the production of BglC suggesting that the expression of *bglC* was not under the control of this aryl β-glucoside. In contrast, BcpE2 was instead maximally produced when salicin was supplied as a unique carbon source and the supply of cellobiose in addition to salicin reduced BcpE2 production to half of this level. When salicin was not supplied in the culture medium, the production levels of BcpE2 dropped to about 16% of its maximal production level. Our results showed that the production of BcpE2 was indeed triggered upon sensing the presence of salicin, one of the substrates for which the enzyme displayed the most efficient catalytic properties.

DISCUSSION

In this work, we reported the structural and biochemical characterization of BcpE2, a GH3-family β-glucosidase of the common scab phytopathogen *S. scabiei*. This protein displayed low similarity compared to biochemically characterized enzymes of this family, indicating that BcpE2 could have novel functional specificities. The crystal structure of BcpE2 revealed the presence of four domains – including a rather uncommon PA14 domain predicted to be involved in substrate specificity – organized around a catalytic pocket, which can accommodate D-Glucose as buried residue. BcpE2 was highly active against a wide variety of plant heterosides mostly containing glucose as carbohydrate residue, with salicin and coniferin as the most efficiently hydrolyzed substrates.

The BcpE2 structure revealed two features likely contributing to its broad substrate specificity, i.e., (i) a wide cavity in the PA14 domain connected to the D-glucose specific subsite (-1), and (ii) the high flexibility of this domain, especially the structure elements defining this cavity (Fig. 4). Three of the four loops not fully defined in the electron density were indeed adjacent to the cavity, which was also surrounded by the residues with the highest B factors. This will, therefore, provide sufficient plasticity to accommodate the various substrates and easy access to efficiently load the substrates and expel the products of the hydrolysis. Except for the aromatic feature of Phe499, which seems to be a characteristic feature of GH3 enzymes, the residues of PA14 defining the cavity were not conserved even among closely related proteins (Fig. S1). This could indicate that the main purpose of the cavity would be to hold the substrate
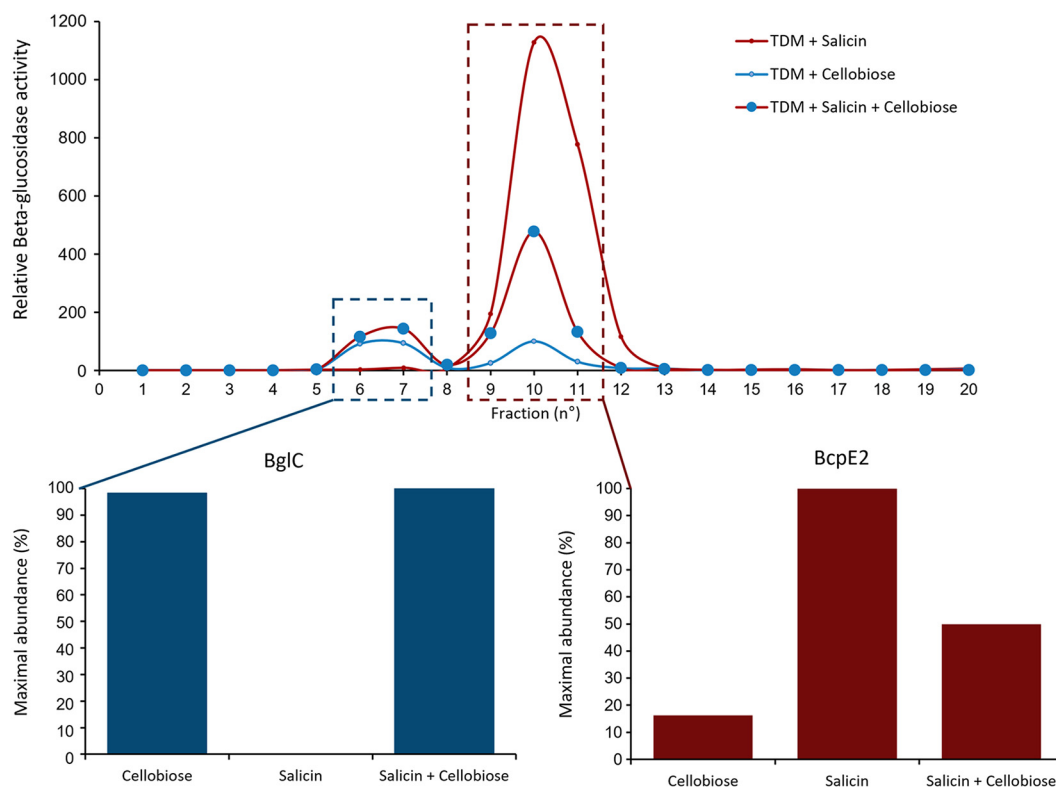
FIG 3 Induction of the respective production of BglC and BcpE2 by cellobiose and salicin. (Top) Relative beta-glucosidase activity in anion-exchange chromatography fractions obtained from the full protein extracts of *S. scabiei* cultured in TDM medium supplemented with salicin (red trait), cellobiose (blue trait), or both substrates (red trait with blue circles). (Bottom) Relative abundance of BglC in the first active peak (fractions 6 to 7) and of BcpE2 in the second active peak (fractions 9 to 11) was determined by targeted proteomics (LC-MRM [Liquid chromatography multiple reaction monitoring] after tryptic digestion of the protein fractions). In each culture condition, the relative protein abundance was reported to the maximal abundance measured for the given protein (see the Materials and methods section for the detailed protocol).

shielded in the active site just a long time enough for hydrolysis to take place, without contributing to the specificity except for setting a size limit.

At this stage, the perhaps most difficult question to answer is: which heteroside could escape hydrolysis by BcpE2? In other words, to what extent can BcpE2 tolerate substrate promiscuity? Glycosylated phytochemicals include phenylpropanoids, cyanogenic glucosides, coumarin heterosides, quinones, monoterpenes, or triterpenes, polyphenols, flavonoids (anthocyanosides, flavanols, isoflavonoids, flavonols, and flavones), monolignols, among many others. Assessing the efficiency of BcpE2 to hydrolyze other substrates with an even wider spectrum of aglycone moieties will likely reveal the extent of its catalytic potential. A single heteroside, amygdalin, was not thoroughly hydrolyzed by BcpE2 (see TLC assay; Fig. 2A), but it was also the only tested compound bearing gentiobiose instead of a glucose molecule as glycone. The gentiobiose disaccharide was poorly degraded by BcpE2, and it was not surprising that amygdalin was not thoroughly hydrolyzed. Despite this, the presence of the aromatic residue in the structure of this cyanogenic glucoside appears to enhance the activity of BcpE2 compared to the hydrolysis of gentiobiose alone. The presence of at least one aromatic cycle in the chemical structure of the heterosides degraded by BcpE2 appeared to be a common feature except for linamarin (Fig. 2A). The fact that this cyanogenic glucoside is also efficiently hydrolyzed by BcpE2 suggests that the presence of an aromatic residue in the aglycone is not a mandatory feature to be accommodated as a substrate.

Why is BcpE2 selected for compensating the loss of BglC? Because cello-oligosaccharides were not natural substrates of BcpE2, the reason why the *bglC*-dependent
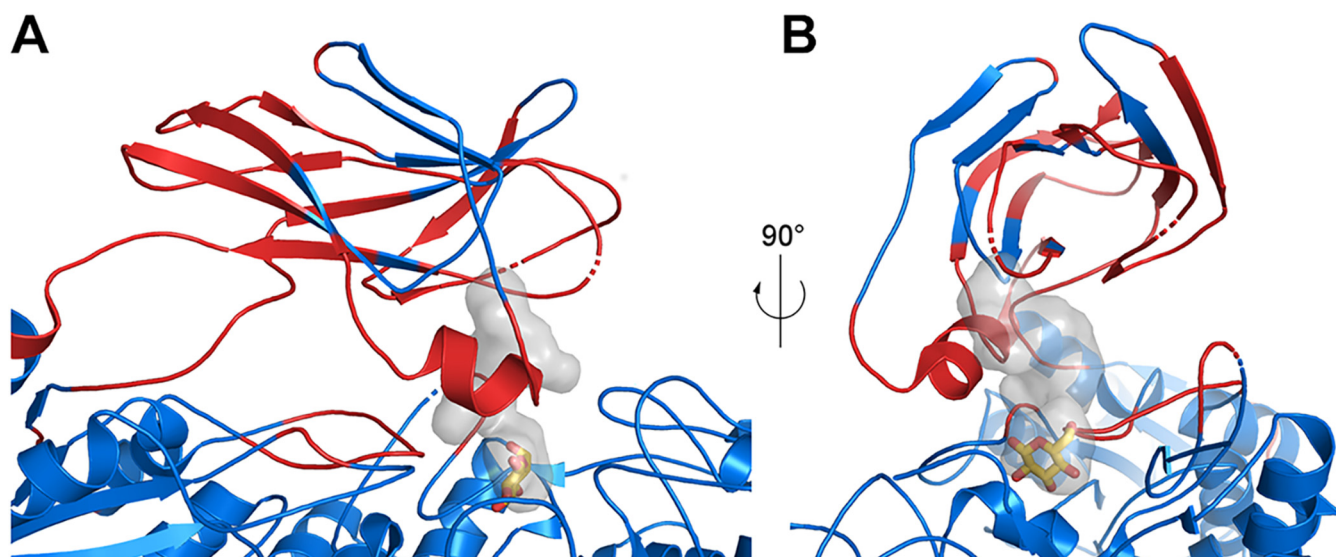
FIG 4 Active site flexibility of BcpE2. (A) Cartoon representation of the BcpE2 active site and the PA14 domain. Loops with missing amino acids are shown as dashed lines. Residues with a B factor of the Cα above 100 Å^2 are in red and the others are in blue. The active site pocket is represented with a transparent surface with the D-glucose molecule in the (+1) subsite from the superimposed KmBglII structure as yellow sticks. (B) Same as in (A) but with a 90° rotation.

mechanism of genetic compensation selected the product of *scab64101* as an alternative β-glucosidase was a complete mystery (20). Considering the discovery of the substrate and enzymatic specificities of BcpE2, it is now easier to understand why the product of this gene was selected to compensate for the loss of *bglC*/BglC. Indeed, we now know that BcpE2 can compensate the impaired cello-oligosaccharide consumption by feeding glycolysis with glucose hydrolyzed from a multitude of plant-derived heterosides, including monolignol glycosides, which were some of the most ubiquitous molecules (Fig. 5). BcpE2 would, therefore, act as a glucose scavenging enzyme and able to provide the most readily metabolized carbon source from a plethora of compounds that *S. scabiei* would encounter during host colonization. For soil-dwelling saprophytic streptomycetes, BcpE2 would be equally important because most of the organic carbon was generated from plant senescence. Indeed, genome mining of streptomycetes revealed that most of them possess an orthologue of BcpE2. It is also striking that BglC and BcpE2 possessed complementary substrate ranges on the tested molecules as the compounds properly hydrolyzed by one are generally badly degraded by the other (Table 2). Overall, the multiplicity of possible substrates for BcpE2, and to a lesser extent for BglC, suggests that these enzymes would be part of a "Swiss army knife" for providing the bacteria the most readily mobilizable sugar from carbon-rich environments. Our results demonstrated that the addition of salicin, one of the best substrates hydrolyzed by BcpE2, as a supplement nutrient in the culture medium strongly induced the production of BcpE2 (Fig. 3). In *S. venezuelae*, a similar situation has been reported where the production of two distinct β-glucosidases responds to either cellobiose or salicin. The enzyme induced by salicin hydrolyzes aryl β-glucosides but is poorly active on cellobiose while the other enzyme is highly active on – and induced by – cellobiose (26). Due to their similarity in terms of catalytic specificity and responsiveness to either cellobiose or salicin, we speculate that these two enzymes of *S. venezuelae* are the orthologues of BglC (VNZ_32510) and BcpE2 (VNZ_10820), which share 70% and 75% of identity with the proteins of *S. scabiei*, respectively. This finding further suggested that this type of GH3 β-glucosidase was not exclusive to *Streptomyces* species that were phytopathogenic.

However, the orthologue of BcpE2 found in *S. scabiei* is most likely involved in additional functions related to pathogenicity as was the case for BglC (10). Indeed, importantly,
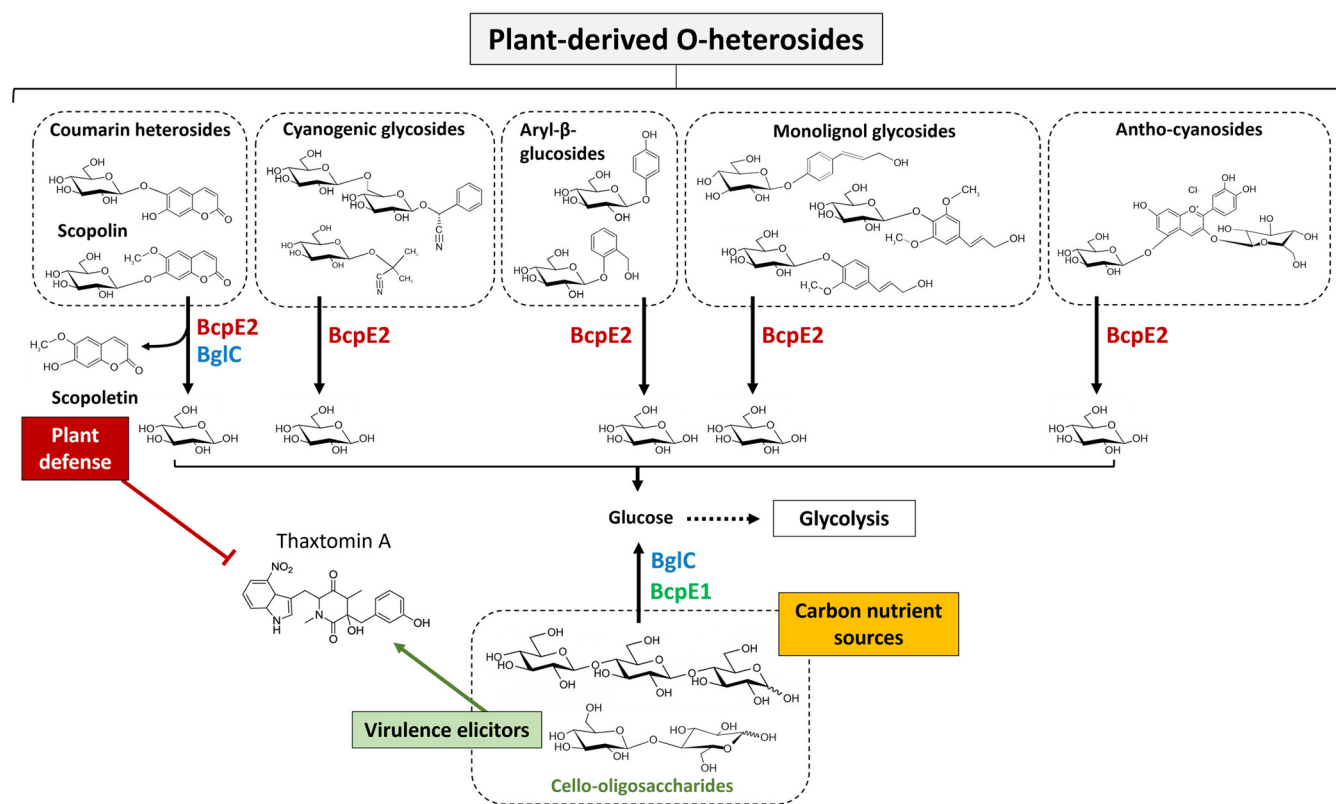
FIG 5 BcpE1 and BcpE2-mediated enzymatic compensation for the loss of BglC. BcpE1 (green) can compensate for the activity of BglC (blue) by generating glucose from the hydrolysis of cello-oligosaccharides cellobiose and cellotriose. BcpE2 (red) can also fuel glycolysis by removing glucose from multiple plant heterosides. In addition, BcpE2 can also compensate for the role of BglC in plant defense mechanism by displaying a substrate inhibition kinetic profile on scopolin, thereby generating the potent thaxtomin A production inhibitor scopoletin.

BcpE2 could also compensate for the loss of a recently discovered function of BglC, i.e., the glucosidase activity on the phytoalexin scopolin (18). *In vitro*, TLC assay revealed that scopolin is the only natural plant compound to be degraded in common by BcpE2 and BglC. Interestingly, the aglycone moiety of scopolin is scopoletin, which has been described as a strong inhibitor of thaxtomin A biosynthesis in *S. scabiei* (19). Because scopoletin and scopolin have been reported to be produced by plant roots or tubers, especially in response to the application of thaxtomin A or under stress conditions such as pathogen infection (19, 27–30), *S. scabiei* is very likely to encounter these molecules upon host colonization. It is therefore tempting to speculate that BglC and BcpE2 are both involved in the management of these compounds and that BcpE2 would be overproduced in the absence of BglC to take over the contribution of the latter.

An important question that remains to be answered: what are the environmental triggers that induce the expression of *bcpE2*? In other words, does the sub-strate promiscuity of BcpE2 correlate with a mechanism of expression control of *bcpE2* sensitive to multiple and dissimilar compounds? We are currently seeking the transcription factor that controls the expression of *bcpE2* orthologues in streptomycetes. Will this transcription factor be able to sense the presence of multiple substrates of BcpE2 or instead only a few structurally similar substrates that would somehow witness the possible presence of plant-heterosides? The answer to this question is crucial for properly understanding the role of this versatile enzyme. In addition, the inactivation of orthologues of *bcpE2* in other model streptomycetes should provide further insight into the importance of this promiscuous enzyme and explain the success of these filamentous bacteria in colonizing plant-derived organic soils.

MATERIALS AND METHODS

Strains, chemicals, and culture conditions. Two strains of *Escherichia coli* were used in the present work: (i) DH5α for routine molecular biology applications, and (ii) BL21(DE3) Rosetta[TM] (Novagen) for heterologous proteins production. Both *E. coli* strains were cultured in LB (BD Difco LB broth) medium supplemented with the appropriate antibiotics (kanamycin [50 μg/mL], chloramphenicol [25 μg/mL]). *Streptomyces scabiei* 87-22 was routinely cultured at 28°C. Tryptic soy broth (TSB, Sigma-Aldrich, 30 g/L) was used for liquid precultures. The modified TDM (thaxtomin-defined medium (15)), the minimal medium was prepared as described in (10), and after autoclaving were supplemented with filter-sterilized carbon sources. The substrates used in this study were purchased from Carbosynth (cellobiose, amygdalin, linamarin, xylobiose, laminaribiose, gentiobiose, salicin, arbutin, and syringin), or Sigma-Aldrich (4-nitrophenyl-β-D-glucopyranoside (pNPβG), esculin, cyanin chloride, 4-methylumbelliferyl β-D-glucopyranoside (4-mug), coniferin (abietin), and *p*-coumaryl alcohol 4-O-glucoside).

Heterologous production of His$_6$-tagged proteins and purification. BcpE2-His$_6$ and His$_6$-BglC were produced in *E. coli* BL21(DE3) Rosetta[TM] transformed with plasmids pBDF004 and pSAJ022, respectively, and purified by nickel affinity chromatography as already described (10, 20). The pure proteins were stored at −20°C and used in HEPES buffer (50 mM, pH 7.5).

Determination of the pH and temperature optima of BcpE2-His$_6$. The β-glucosidase activity was typically determined by the degradation of 4-Nitrophenyl-β-D-glucopyranoside (pNPβG). Ninety-five microliters of a determined BcpE2-His$_6$ concentration diluted in HEPES buffer (50 mM, pH 7.5) were mixed with 5 μL of pNPβG (20 mM). After incubation at 25°C, the reaction was stopped by the addition of 100 μL of Na$_2$CO$_3$ (2 M). The release of *para*-nitrophenol was monitored by measuring the absorbance at 405 nm with a TECAN Infinite 200 PRO. The temperature optimum was determined by varying the incubation temperature from 5 to 60°C with 5°C increments. The pH optimum was determined by varying the pH of the reaction with the use of 3 distinct buffers, i.e., (i) MES buffer (50 mM) for pH ranging between 5.0 and 6.5, (ii) HEPES buffer (50 mM) for pH ranging between 7.0 and 8.5, and (iii) CHES buffer (50 mM) for pH ranging between 9.0 and 10.0. The measured activity was reported to the maximal value obtained in each experiment which was set to 100%. The results are in Fig. S3.

TLC for hydrolysis of cello-oligosaccharides. Semiquantitative substrate degradation was assessed by thin-layer chromatography (TLC). Reactions were carried out with the BcpE2-His$_6$ and His$_6$-BglC enzymes (1 μM) and the substrates (5 mM) in HEPES 50 mM pH 7.5 at 40°C for 10 min. At the end of the reaction, the mixture was incubated for 5 min in a boiling water bath to inactivate the enzyme. 1-μL samples of the inactivated reaction mixtures were spotted next to undigested standards on aluminum-backed TLC plates (silica gel matrix, Sigma-Aldrich) and thoroughly dried. The protocol, adapted from (31), consisted in eluting the loaded TLC plate in a TLC chamber filled with an elution buffer (chloroform-methanol-acetic acid-water [50:50:15:5 (vol/vol)]). After air-drying the eluted plate, sulfuric acid (5%) in ethanol was sprayed onto the TLC plate and the excess liquid was drained. The revelation was conducted by heating the TLC plate on a hot plate.

Determination of kinetic parameters for BcpE2-His$_6$. The hydrolysis of nonchromogenic substrates for β-glucosidases was followed by glucose quantification, either by HPLC (see HPLC quantification of glucose) or with the D-Glucose HK assay kit (Megazyme) following the microplate procedure. BcpE2-His$_6$ was mixed with the substrate at variable concentrations in HEPES 50 mM pH 7.5, and the incubation was conducted at 40°C for 4 min. The reaction was terminated by a 5-min incubation in a boiling water bath. At least 10 concentrations – if possible distributed around the K$_m$ value – were tested in triplicate for each substrate to estimate initial velocity values. The obtained data – initial velocity (V$_i$, mM/min) in function of substrate concentration ([S], mM) – were fitted to the Henri-Michaelis-Menten equation $V_i = (V_{max} \times [S])/(K_m + [S])$ using the GraphPad Prism (version 9.2.0) software. K$_m$ (mM), V$_{max}$ (mM/min), k$_{cat}$ (s^{-1}) and the specificity constant (k$_{cat}$/K$_m$ [mM^{-1} s^{-1}]) were determined for each substrate. Substrate inhibition constants were also determined with GraphPad Prism following the equation, $V_i = (V_{max} \times [S])/(K_m + [S] \times [1 + [S]/K_i])$.

HPLC quantification of glucose. Glucose quantification was performed on a Waters HPLC device composed of a Separation Module (e2695) and a refractive index (RI) detector (2414) set at 50°C. 35 μL of glucose-containing samples from terminated reactions were injected into an Aminex HPX-87P (Bio-Rad) column (300 × 7.8 mm) and placed in an oven at 80°C. An isocratic flow of milli-Q water was conducted for 20 min at a flow rate of 0.6 mL/min. The RI detector was set on channel 410 and sensitivity 256, and the measurements were expressed in RI units (RIU). The peak areas associated with glucose (R$_t$ = 11.6 min) were integrated and converted into glucose concentrations based on a linear standard curve ranging from 0.1 ng/μL to 400 ng/μL following the equation: y = 644.09x − 3170.4 (y being the Peak area (μV × sec) and x being the glucose amount (ng)/10 μL injected).

Crystallization and structure determination of BcpE2-His$_6$. BcpE2 was concentrated to 17.4 mg/mL in HEPES 50 mM pH 7.5 and crystallized using the sitting-drop vapor diffusion method. 0.2 μL of protein was mixed with 0.2 μL of precipitant solution (methylpentane-2,4-diol [MPD] 45%, Tris-HCl 0.1 M pH 8.5 and 0.2 M ammonium acetate) and crystals grew at room temperature. The crystals were transferred into a cryoprotectant solution containing 50% MPD and 50% polyethylene glycol 400 before flash-freezing in a liquid nitrogen bath. Diffraction data were collected at the Soleil Synchrotron Proxima 2a beamline (Paris). Data were integrated and scaled using XDS (X-ray Detector Software (32)). Initial phases were obtained by molecular replacement using the structure of DesR from *S. venezuelae* as a search model (PDB accession no. 4I3G (22)) using a Phaser (33). The structure was built with Coot (Crystallographic object-oriented toolkit (34)) and refined with (BUSTER refine (35)). The figures were prepared using PyMOL (PyMOL Molecular Graphics System, Version 2.4.1 Enhanced for Mac OS X, Schrödinger, LLC.).

Computational tools. The structure-based alignment was built using the MultAlin-ESPript (3.0) combined tool (36, 37) using the structure of BcpE2 (PDB accession no. 7PPJ) as a reference for positioning

secondary structure elements. The sequences of seven additional characterized GH3 enzymes were included in the alignment (Table S1).

The phylogenetic tree was constructed using the phylogeny.fr tool with the "One Click" mode (38). The repertoire of characterized bacterial and eukaryotic GH3 proteins was obtained from the CAZy database (accessed on August 27th, 2021) and the amino acid sequences obtained were subsequently used in a BLASTp analysis against BcpE2 to select the appropriate proteins for the phylogenetic analysis (Table S1).

The search for PA14 domains was carried out using the MOTIF Search tool (Genome.jp) on the characterized bacterial and eukaryotic GH3 proteins from the CAZy database. The scan for motifs included the Pfam and NCBI-CDD databases in which the pfam07691 or 400161 and 214807 PSSM-Ids were searched for, respectively. In addition, the ScanProsite tool (Expasy) was used on the same amino acid sequences searching for the PA14 (PROSITE entry: PS51820) motif. A manual inspection was conducted to search for the presence of a PA14 domain in the closest GH3s (compared to BcpE2) that were not selected by the search tool. This inspection consisted of a comparison of the predicted secondary structures in the appropriate region of the proteins.

Determination of the intracellular β-glucosidase activity. Anion exchange chromatography (AXC) to obtain fractions of intracellular β-glucosidases was performed similarly to the method described in (20) with protein extracts prepared from cultures of *S. scabiei* 87-22 in TDM supplemented with salicin (0.1%) and/or cellobiose (0.1%). Briefly, 48-h precultures in TSB were washed twice in TDM without a carbon source. After resuspension of the mycelium under the conditions described above, the culture was carried out for 7.5 h at 28°C. After centrifugation, the mycelium pellet was resuspended in HEPES buffer (50 mM, pH 7.5) and disrupted with an Avestin Emulsiflex C3 homogenizer (3 lysis cycles). The soluble fraction was obtained by centrifugation of the lysed cell suspension and filtering (0.22 μm cutoff) of the supernatant. Using an NGC Quest 10 (Bio-Rad) and a HiTrap^{TM} Q HP column (GE health care), protein fractions were generated by elution with a linear NaCl gradient (0 to 1 M). The β-glucosidase activity of each fraction was determined by the standard assay using pNPβG as the substrate (as described in (10, 20)) and reported to the estimated protein content (absorbance at 280 nm [A_{280}]) of the fraction. These relative activities were then normalized to the maximal activity observed in the second peak (corresponding to BcpE2) of the TDM + cellobiose condition.

Targeted proteomics analysis. Collection of fractions by anion-exchange chromatography and subsequent liquid chromatography multiple reaction monitoring (LC-MRM) to monitor the relative abundance of BglC and BcpE2 in protein fractions was performed as previously described (20, 39) and detailed in Table S2.

Data availability. The crystallographic structure of BcpE2 has been deposited in the Protein Data Bank with accession number 7PJJ.

SUPPLEMENTAL MATERIAL

Supplemental material is available online only.

FIG S1, DOCX file, 2.6 MB.
FIG S2, DOCX file, 0.4 MB.
FIG S3, DOCX file, 0.1 MB.
TABLE S1, DOCX file, 0.1 MB.
TABLE S2, DOCX file, 0.03 MB.

REFERENCES

1. Hodgson DA. 2000. Primary metabolism and its control in streptomycetes: a most unusual group of bacteria. Adv Microb Physiol 42:47–238. https://doi.org/10.1016/s0065-2911(00)42003-5.
2. Book AJ, Lewin GR, McDonald BR, Takasuka TE, Wendt-Pienkowski E, Doering DT, Suh S, Raffa KF, Fox BG, Currie CR. 2016. Evolution of high cellulolytic activity in symbiotic streptomyces through selection of expanded gene content and coordinated gene expression. PLoS Biol 14:e1002475. https://doi.org/10.1371/journal.pbio.1002475.
3. Lewin GR, Carlos C, Chevrette MG, Horn HA, McDonald BR, Stankey RJ, Fox BG, Currie CR. 2016. Evolution and ecology of actinobacteria and their bioenergy applications. Annu Rev Microbiol 70:235–254. https://doi.org/10.1146/annurev-micro-102215-095748.

4. Chater KF, Biró S, Lee KJ, Palmer T, Schrempf H. 2010. The complex extracellular biology of Streptomyces. FEMS Microbiol Rev 34:171–198. https://doi.org/10.1111/j.1574-6976.2009.00206.x.

5. Lakhundi S, Siddiqui R, Khan NA. 2015. Cellulose degradation: a therapeutic strategy in the improved treatment of Acanthamoeba infections. Parasit Vectors 8:23. https://doi.org/10.1186/s13071-015-0642-7.

6. Takasuka TE, Book AJ, Lewin GR, Currie CR, Fox BG. 2013. Aerobic deconstruction of cellulosic biomass by an insect-associated Streptomyces. Sci Rep 3:1030. https://doi.org/10.1038/srep01030.

7. Jourdan S, Francis IM, Kim MJ, Salazar JJC, Planckaert S, Frère J-M, Matagne A, Kerff F, Devreese B, Loria R, Rigali S. 2016. The CebE/MsiK transporter is a doorway to the cello-oligosaccharide-mediated induction of streptomyces scabies pathogenicity. Sci Rep 6:27144. https://doi.org/10.1038/srep27144.

8. Schlösser A, Jantos J, Hackmann K, Schrempf H. 1999. Characterization of the binding protein-dependent cellobiose and cellotriose transport system of the cellulose degrader Streptomyces reticuli. Appl Environ Microbiol 65:2636–2643. https://doi.org/10.1128/AEM.65.6.2636-2643.1999.

9. Schlösser A, Kampers T, Schrempf H. 1997. The Streptomyces ATP-binding component MsiK assists in cellobiose and maltose transport. J Bacteriol 179:2092–2095. https://doi.org/10.1128/jb.179.6.2092-2095.1997.

10. Jourdan S, Francis IM, Deflandre B, Tenconi E, Riley J, Planckaert S, Tocquin P, Martinet L, Devreese B, Loria R, Rigali S. 2018. Contribution of the β-glucosidase BglC to the onset of the pathogenic lifestyle of Streptomyces scabies. Mol Plant Pathol 19:1480–1490. https://doi.org/10.1111/mpp.12631.

11. Spiridonov NA, Wilson DB. 2001. Cloning and biochemical characterization of BglC, a beta-glucosidase from the cellulolytic actinomycete Thermobifida fusca. Curr Microbiol 42:295–301. https://doi.org/10.1007/s002840110220.

12. Deflandre B, Stulanovic N, Planckaert S, Anderssen S, Bonometti B, Karim L, Coppieters W, Devreese B, Rigali S. 2022. The virulome of Streptomyces scabiei in response to cello-oligosaccharide elicitors. Microb Genom 8:e000760. https://doi.org/10.1099/mgen.0.000760.

13. Wach MJ, Krasnoff SB, Loria R, Gibson DM. 2007. Effect of carbohydrates on the production of thaxtomin A by Streptomyces acidiscabies. Arch Microbiol 188:81–88. https://doi.org/10.1007/s00203-007-0225-x.

14. Jourdan S, Francis IM, Deflandre B, Loria R, Rigali S. 2017. Tracking the subtle mutations driving host sensing by the plant pathogen streptomyces scabies. mSphere 2:e00367-16. https://doi.org/10.1128/mSphere.00367-16.

15. Johnson EG, Joshi MV, Gibson DM, Loria R. 2007. Cello-oligosaccharides released from host plants induce pathogenicity in scab-causing Streptomyces species. Physiological and Molecular Plant Pathology 71:18–25. https://doi.org/10.1016/j.pmpp.2007.09.003.

16. Francis IM, Jourdan S, Fanara S, Loria R, Rigali S. 2015. The cellobiose sensor CebR is the gatekeeper of Streptomyces scabies pathogenicity. mBio 6:e02018. https://doi.org/10.1128/mBio.02018-14.

17. Planckaert S, Jourdan S, Francis IM, Deflandre B, Rigali S, Devreese B. 2018. Proteomic response to thaxtomin phytotoxin elicitor cellobiose and to deletion of cellulose utilization regulator CebR in Streptomyces scabies. J Proteome Res 17:3837–3852. https://doi.org/10.1021/acs.jproteome.8b00528.

18. Deflandre B, Rigali S. 2021. Old enzyme, new role: the β-glucosidase BglC of Streptomyces scabiei interferes with the plant defense mechanism by hydrolyzing scopolin. Biophysica 2:1–7. https://doi.org/10.3390/biophysica2010001.

19. Lerat S, Babana AH, El Oirdi M, El Hadrami A, Daayf F, Beaudoin N, Bouarab K, Beaulieu C. 2009. Streptomyces scabiei and its toxin thaxtomin A induce scopoletin biosynthesis in tobacco and Arabidopsis thaliana. Plant Cell Rep 28:1895–1903. https://doi.org/10.1007/s00299-009-0792-1.

20. Deflandre B, Thiébaut N, Planckaert S, Jourdan S, Anderssen S, Hanikenne M, Devreese B, Francis I, Rigali S. 2020. Deletion of bglC triggers a genetic compensation response by awakening the expression of alternative beta-glucosidase. Biochim Biophys Acta Gene Regul Mech 1863:194615. https://doi.org/10.1016/j.bbagrm.2020.194615.

21. Yoshida E, Hidaka M, Fushinobu S, Koyanagi T, Minami H, Tamaki H, Kitaoka M, Katayama T, Kumagai H. 2010. Role of a PA14 domain in determining substrate specificity of a glycoside hydrolase family 3

β-glucosidase from Kluyveromyces marxianus. Biochem J 431:39–49. https://doi.org/10.1042/BJ20100351.

22. Zmudka MW, Thoden JB, Holden HM. 2013. The structure of DesR from Streptomyces venezuelae, a β-glucosidase involved in macrolide activation. Protein Sci 22:883–892. https://doi.org/10.1002/pro.2204.

23. Yoshida E, Hidaka M, Fushinobu S, Koyanagi T, Minami H, Tamaki H, Kitaoka M, Katayama T, Kumagai H. 2009. Purification, crystallization and preliminary X-ray analysis of beta-glucosidase from Kluyveromyces marxianus NBRC1777. Acta Crystallogr Sect F Struct Biol Cryst Commun 65:1190–1192. https://doi.org/10.1107/S1744309109042948.

24. Mahasenan KV, Batuecas MT, De Benedetti S, Kim C, Rana N, Lee M, Hesek D, Fisher JF, Sanz-Aparicio J, Hermoso JA, Mobashery S. 2020. Catalytic cycle of glycoside hydrolase BglX from Pseudomonas aeruginosa and its implications for biofilm formation. ACS Chem Biol 15:189–196. https://doi.org/10.1021/acschembio.9b00054.

25. Hrmova M, Streltsov VA, Smith BJ, Vasella A, Varghese JN, Fincher GB. 2005. Structural rationale for low-nanomolar binding of transition state mimics to a family GH3 β-d-glucan glucohydrolase from barley. Biochemistry 44:16529–16539. https://doi.org/10.1021/bi0514818.

26. Chatterjee S, Vining LC. 1982. Glucose suppression of beta-glucosidase activity in a chloramphenicol-producing strain of Streptomyces venezuelae. Can J Microbiol 28:593–599. https://doi.org/10.1139/m82-088.

27. Bednarek P, Schneider B, Svatos A, Oldham NJ, Hahlbrock K. 2005. Structural complexity, differential response to infection, and tissue specificity of indolic and phenylpropanoid secondary metabolism in Arabidopsis roots. Plant Physiol 138:1058–1070. https://doi.org/10.1104/pp.104.057794.

28. Clarke DD. 1973. The accumulation of scopolin in potato tissue in response to infection. Physiological Plant Pathology 3:347–358. https://doi.org/10.1016/0048-4059(73)90006-4.

29. Nolte P, Secor GA, Gudmestad NC, Henningson PJ. 1993. Detection and identification of fluorescent compounds in potato tuber tissue with corky patch syndrome. American Potato J 70:649–666. https://doi.org/10.1007/BF02849154.

30. Ward JL, Baker JM, Llewellyn AM, Hawkins ND, Beale MH. 2011. Metabolomic analysis of Arabidopsis reveals hemiterpenoid glycosides as products of a nitrate ion-regulated, carbon flux overflow. Proc Natl Acad Sci U S A 108:10762–10767. https://doi.org/10.1073/pnas.1018875108.

31. Gao J, Wakarchuk W. 2014. Characterization of five β-glycoside hydrolases from Cellulomonas fimi ATCC 484. J Bacteriol 196:4103–4110. https://doi.org/10.1128/JB.02194-14.

32. Kabsch W. 2010. XDS. Acta Crystallogr D Biol Crystallogr 66:125–132. https://doi.org/10.1107/S0907444909047337.

33. McCoy AJ, Grosse-Kunstleve RW, Adams PD, Winn MD, Storoni LC, Read RJ. 2007. Phaser crystallographic software. 4. J Appl Crystallogr 40:658–674. https://doi.org/10.1107/S0021889807021206.

34. Emsley P, Lohkamp B, Scott WG, Cowtan K. 2010. Features and development of Coot. Acta Crystallogr D Biol Crystallogr 66:486–501. https://doi.org/10.1107/S0907444910007493.

35. Blanc E, Roversi P, Vonrhein C, Flensburg C, Lea SM, Bricogne G. 2004. Refinement of severely incomplete structures with maximum likelihood in BUSTER-TNT. Acta Crystallogr D Biol Crystallogr 60:2210–2221. https://doi.org/10.1107/S0907444904016427.

36. Corpet F. 1988. Multiple sequence alignment with hierarchical clustering. Nucleic Acids Res 16:10881–10890. https://doi.org/10.1093/nar/16.22.10881.

37. Robert X, Gouet P. 2014. Deciphering key features in protein structures with the new ENDscript server. Nucleic Acids Res 42:W320–324. https://doi.org/10.1093/nar/gku316.

38. Dereeper A, Guignon V, Blanc G, Audic S, Buffet S, Chevenet F, Dufayard J-F, Guindon S, Lefort V, Lescot M, Claverie J-M, Gascuel O. 2008. Phylogeny.fr: robust phylogenetic analysis for the non-specialist. Nucleic Acids Res 36:W465–469. https://doi.org/10.1093/nar/gkn180.

39. Planckaert S, Deflandre B, de Vries A-M, Ameye M, Martins JC, Audenaert K, Rigali S, Devreese B. 2021. Identification of novel rotihibin analogues in Streptomyces scabies, including discovery of its biosynthetic gene cluster. Microbiol Spectr 9:e0057121. https://doi.org/10.1128/Spectrum.00571-21.